Anthropocene 7 (2014) 16–29

Contents lists available at ScienceDirect

Anthropocene

journal homepage: www.elsevier.com/locate/ancene

Quantifying an early signature of the industrial revolution from lead concentrations and isotopes in soils of Pennsylvania, USA

Lin Ma [a,*], Jasper Konter [a], Elizabeth Herndon [b], Lixin Jin [a], Grit Steinhoefel [c], Diego Sanchez [a], Susan Brantley [b,c]

[a] Department of Geological Sciences, University of Texas at El Paso, El Paso, TX 79968, United States
[b] Department of Geosciences, Pennsylvania State University, University Park, PA 16802, United States
[c] Earth and Environmental Systems Institute, Pennsylvania State University, University Park, PA 16802, United States

ARTICLE INFO

Article history:
Received 17 June 2013
Received in revised form 15 December 2014
Accepted 17 December 2014
Available online 30 December 2014

Keywords:
Heavy metal pollution
Industrial revolution
Pb isotopes and concentration
Soils
Critical zone

ABSTRACT

During the early industrial revolution, mining and smelting of ores and coal combustion released significant amounts of lead (Pb) into the atmosphere. While many researchers have documented high Pb concentrations in topsoils due to gasoline combustion between 1940s and 1980s, little work has focused on the extent of Pb and other heavy metal deposition into soils during the early industrial period. Here, we report Pb, cadmium (Cd), and zinc (Zn) concentrations and Pb isotope ratios of soils, sediments, parent bedrock, and waters collected from a small, currently pristine watershed (Shale Hills Critical Zone Observatory) in Pennsylvania (United States of America). Our results show that Pb in the soil comprises an addition profile, i.e. more Pb is present in the soil than is present in the equivalent parent bedrock. All three investigated soil profiles at Shale Hills on the same hillslope have Pb inventories (~400–600 $\mu g\ cm^{-2}$) attributed to atmospheric deposition. Cd and Zn concentrations in these soils show similar addition profiles due to atmospheric deposition. Based on Pb isotopic ratios, the most likely source of the added Pb is coal burning and ore smelting during local iron production in the early 19th century, roughly coincident with the construction of the U.S. transcontinental railroad. Mass balance and diffusive transport modeling were used to quantify Pb deposition rates and redistribution. These model results are consistent with the hypothesis that from ~1850s to 1920s, coal burning and ore smelting in local iron blasting furnaces significantly increased the local Pb emissions so that Pb deposition rates in soils were in the range of 6–10 $\mu g\ cm^{-2}\ yr^{-1}$. These values are comparable to Pb deposition rates found in other areas with early and intensive industrial activities (e.g. since the ~1860s in Australia). Our new Pb, Cd, and Zn concentrations and Pb isotope results, in combination with the previously observed manganese (Mn) enrichment at Shale Hills, document that early industrial point sources contaminated local soils with metals that remain even today in topsoils with large sorption capacities. Where these metals are retained, their depth profiles provide a mean to infer the history of metal additions and redistributions.

Introduction

Since the industrial revolution, anthropogenic factors have been dominant in a way that humans are changing the Earth's surface at much faster rates than many natural processes (Caldeira et al., 2004). For example, human activities have significantly increased the metal emissions of lead (Pb), copper (Cu), zinc (Zn), cadmium (Cd) and manganese (Mn) to the atmosphere, and these metals are subsequently deposited back to Earth's surface, disrupting their natural biogeochemical cycles (Lantzy and Mackenzie, 1979; Galloway et al., 1982; Nriagu and Pacyna, 1988; Dudka and Adriano, 1997; Reuer and Weiss, 2002; Taylor et al., 2010; Cloquet et al., 2006; Komarek et al., 2008; Rauch and Pacyna, 2009).

Perhaps the best studied of these metals is Pb – cycling of this element in terrestrial and marine environments has been dominated by anthropogenic factors. In fact, metal production from Pb-rich sulfides has released anthropogenic Pb to the environment since ~5000 yr BP (Reuer and Weiss, 2002). During the industrial revolution, the extent of atmospheric Pb emission increased significantly due to increasing demands for metals and energy (Edgington and Robbins, 1976). During the early period of the industrial revolution (i.e. in the 1800s), activities such as mining and smelting of ores and coal combustion became major sources of Pb into the environment (Reuer and Weiss, 2002). The

* Corresponding author. Tel.: +1 915 747 5218.
E-mail address: lma@utep.edu (L. Ma).

http://dx.doi.org/10.1016/j.ancene.2014.12.003
2213-3054/

dominant source of anthropogenic Pb to the atmosphere from the 1940s to 1980s was leaded gasoline, which caused widespread emission of Pb into the environment (Nriagu and Pacyna, 1988). Lake and estuary sediments, ice cores, lichens, and corals have all been used to reconstruct the history of industrial Pb deposition. These types of samples generally can store metals derived from atmospheric inputs (e.g., Edgington and Robbins, 1976; Graney et al., 1995; Reuer and Weiss, 2002; Marcantonio et al., 2002; Lima et al., 2005; Hissler et al., 2008; Geagea et al., 2008; Kelly et al., 2009). Several dating techniques (e.g., using sedimentation rates, coral growth layers, and radioactive isotope chronometers) have also been applied to such samples to establish the time frames of metal deposition and to quantify the deposition rates (e.g., Graney et al., 1995; Lima et al., 2005; Kelly et al., 2009).

Soils are also sinks for atmospheric metal deposition. However, the geographic extent and pollutant sources of industrial metal loading to soils have not been evaluated extensively (e.g., Markus and McBratney, 2001). One of the reasons is that soils, as open systems, receive metals from atmospheric deposition and from weathering of bedrock while losing these metals through chemical weathering and physical erosion processes (e.g., Watmough et al., 2004; Steinnes and Friedland, 2005). Furthermore, metals such as Pb can be redistributed within the soil column. It has thus been rare to reconstruct the history of metal deposition from soil records. Only a few such attempted reconstructions appear in the literature. In these, models that calculate Pb mass balance and incorporate Pb transport in soil profiles have been used to understand the history of Pb addition and redistribution in the uppermost layers of soils (e.g., Miller and Friedland, 1994; He and Walling, 1997; Kaste et al., 2003, 2007; Brantley and Lebedeva, 2011; Drivas et al., 2011). Such soil studies should be most successful in illuminating our understanding of metal deposition in field sites where the important hydrologic, geomorphologic, and biogeochemical processes have been investigated.

In this study, we investigate local Pb loading history in soils from a well-studied, relatively pristine, small temperate watershed in Pennsylvania by combining Pb concentration and isotope measurements with mass balance models. To decipher processes related to soil formation and disturbance, it is necessary to integrate soil, geologic, ecologic, and hydrologic data. We therefore focus our study on the Susquehanna Shale Hills Critical Zone Observatory (or Shale Hills), one of ten Critical Zone Observatories (CZOs) in the United States (www.criticalzone.org). This site offers multidisciplinary data encompassing many of the relevant processes within the critical zone, i.e., the layer that extends from the top of the vegetation canopy to the depths of ground water (e.g. Brantley et al., 2007).

Background

Pb stable isotopes (^{204}Pb, ^{206}Pb, ^{207}Pb and ^{208}Pb) have been widely used to trace Pb sources. The primary Pb ores around the world are characterized by an exceptionally large range of Pb isotope signatures. Such Pb ores are generally less radiogenic than Pb found in common rocks and minerals Hence, Pb isotopes have been widely used as an environmental tracer for separating anthropogenic Pb (e.g. derived from Pb ores) from natural Pb derived from mineral weathering (Erel et al., 1994; Graney et al., 1995; Reuer and Weiss, 2002; Blum and Erel, 2004).

The Shale Hills watershed experienced relatively minimal human disturbance in the past compared to many other watersheds in the industrialized region of northeastern United States. However, detailed soil characterization has revealed the presence of unusually high levels of Mn in surface soils (Herndon et al., 2011). In that study, a mass balance calculation based on Mn concentrations in different geochemical pools (bedrock, soil, precipitation, and soil pore water) demonstrated that atmospheric deposition at Shale Hills is the main source of the Mn contamination. Herndon et al. (2011) further hypothesized that the Mn contamination can be attributed to (1) iron production in the 19th century in Pennsylvania; (2) modern steel plants and coal-burning power plants that are located upwind; and (3) contributions from recent gasoline combustion. Contribution from Mn from the iron ore smelting (from 1850 to 1920) was highlighted as particularly important. Indeed, during the peak of iron production in the mid-1800s, there were approximately 90 operational furnaces and forges in Central Pennsylvania (Eggert, 1994). High levels of Mn emission to the air during this time period could have been due to (i) burning of coals to drive the furnaces, (ii) release of Mn from the smelting of the iron ore itself, or (iii) release of Mn from combustion of the Mn-rich limestone used as a fluxing agent. Herndon et al. (2011) also showed historical datasets and hypothesized that over half of the soils surveyed in Pennsylvania and in many industrialized areas of North America and Europe are enriched in Mn, Pb and Cd. In this study, we combine Pb concentrations and Pb isotopic ratios with mass balance and diffusive transport models to investigate the sources of Pb in soil profiles in the local Shale Hills area.

Study area

The Shale Hills CZO, a small, forested, and relatively pristine 8-ha watershed, was established in Huntington County, Pennsylvania (Fig. 1; http://www.czo.psu.edu/) for integrated research (Fig. 1b). The CZO is located in the northern part of the Appalachian Mountains. Geographic, geochemical, hydrological and soil studies have been conducted at Shale Hills since the 1970s (Lynch, 1976; Lynch and Corbett, 1985; Duffy and Cusumano, 1998; Lin, 2006; Lin et al., 2006; Qu and Duffy, 2007; Jin et al., 2010, 2011a,b; Ma et al., 2010, 2011a,b, 2013; Yesavage et al., 2012). The site information is briefly summarized below.

The climate at Shale Hills is temperate and humid, with a mean annual temperature of 10 °C and mean annual precipitation of 107 cm (NOAA, 2007). Rainfall is spread over the year and the snowfall season lasts from December to March. The prevailing wind direction is from west to east (Lima et al., 2005).

The catchment has an average local relief of 30 m and a 1st-order stream flows through the central valley floor from east to west (Lynch, 1976; Lin, 2006) (Fig. 1). The catchment is largely vegetated by deciduous trees (maple, oak, and beech) as well as hemlock and pine (Lin, 2006; Naithani et al., 2013). The catchment experienced two significant perturbations in the geologically recent past: a perturbation from peri-glacial to modern conditions (~15 kyr; Gardner et al., 1991) that has affected long-term regolith formation processes (Ma et al., 2010, 2013), and clearing of forests during colonial occupation that represents a short-term disturbance to local ecology and the environment.

The Silurian bedrock at Shale Hills, known as the Rose Hill Formation within the Clinton group, is dominated by organic-poor and Fe-rich shale (~0.05 wt.% total carbon and ~5.5 wt.% of total Fe; Jin et al., 2010) with rare interbedded carbonate- or sand-rich units (Folk, 1960; Lynch, 1976; Lynch and Corbett, 1985). In fact, Fe-rich sections of the Clinton group were mined as iron ores and used in the local pig iron furnaces around Shale Hills in the early 1800s (Eggert, 1994). Carbonate minerals, e.g., ankerite, have been observed in samples recovered from a borehole drilled at the northern ridge from ~20 m below the surface (DC1) (Fig. 1b). In the upper, carbonate-poor portion, the shale is composed predominantly of illite (58 wt.%), quartz (30 wt.%), chlorite + vermiculite + hydroxyl-interlayered vermiculite (referred to here as "chlorite", 11 wt.%), and trace amounts of feldspar (plagioclase and K-feldspar), anatase (TiO_2), pyrite, Fe-oxides (magnetite and hematite) and zircon (Jin et al., 2010; Brantley et al., 2013). No Pb-rich minerals have been observed in the bedrock.

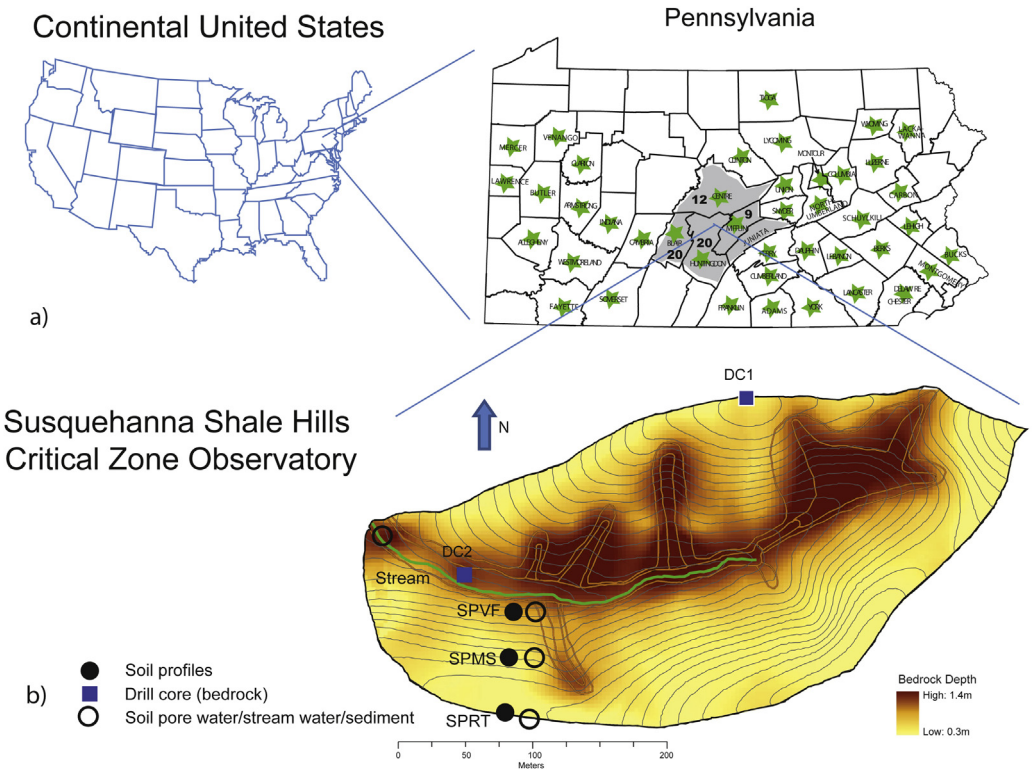

Fig. 1. (a) Location of Susquehanna Shale Hills Critical Zone Observatory in Pennsylvania. Green stars highlight the counties with furnaces for iron and steel manufacturing in Pennsylvania in 1850s. Most of the furnaces used coal or "coke" as fuels. Gray area indicates the "Juniata Iron Region" consisting of Blair, Centre, Clinton, Huntingdon, and Mifflin Counties. This region produced more iron than any other county in the nation in the 19th century (Eggert, 1994). The numbers of major iron furnaces in this region were indicated (from Pennsylvania Iron Furnace Source Book; http://paironworks.rootsweb.ancestry.com) (b) Sample locations in the Shale Hills catchment (modified after Lin et al. (2006) and Ma et al. (2010, 2011a)). Background color indicates soil thickness (Lin et al., 2006); gray lines indicate topographic contours (2 m interval); DC1 and DC2 are the drill core sites where deep shale was sampled and characterized as parent materials (Jin et al., 2010). Soil cores SPRT, SPMS, and SPVF comprise a relatively planar hillslope transect (a catena). Natural water samples include soil pore waters (sampled from lysimeter nests at the SPRT, SPMS, and SPVF locations) and stream waters (at the outlet of the catchment). One stream sediment sample was collected from the outlet of the stream.

Soil thickness increases from ~0.3 m at the ridge top to greater than 3 m in the valley floor and in swales (Fig. 1b). Chemical weathering reactions in the Shale Hills soils are dominated by clay transformations: illite and "chlorite" weather to produce vermiculite, hydroxyl-interlayered vermiculite, and kaolinite (Jin et al., 2010). U-series isotope activity ratios were measured and modeled to determine the timescales of chemical weathering involved at Shale Hills (Ma et al., 2010, 2013). Along a planar transect on the southern slope (Fig. 1b), the U-series isotopes of the thin soils (~30 cm) at the ridge top are interpreted to show that the soils have formed at high rates (~45 ± 12 m/Myr). If we assume that regolith formation and erosion rates are the same, this corresponds to a relatively short residence time for the soil particles within the soil profile at the ridge (~7 ± 2 kyr). Indeed, comparison of U-series and ^{10}Be isotope measurements suggests that the regolith formation and erosion rates agree within error for the ridge-top site at Shale Hills (Ma et al., 2013; West et al., 2013). Thick soils (~70 cm) at the middle slope and valley floor are consistent with slower soil formation rates (~17 ± 14 m/Myr) and much longer residence times (~40 ± 30 kyr). Note that these timescales are much longer than the time periods (e.g. the last 200 years) during which disturbances by human activities were important.

Samples, experimental protocols and analytical methods

Sample collection

Major element, trace element, mineralogy, U, Fe, Mg and Be isotopic analyses for soil and water samples at Shale Hills have been previously reported (e.g., Jin et al., 2010, 2011a,b; Ma et al., 2010, 2011a,b, 2013; West et al., 2011; Yesavage et al., 2012). We focus here on the Pb isotope compositions and concentrations of soil profiles along the "planar" transect from the southern slope of the catchment where most of the prior geochemical work has been focused (Fig. 1b). Three sites were analyzed along the hillslope (southern planar ridge top: SPRT; middle slope: SPMS; valley floor: SPVF). A 25 m deep drill core (DC1) on the northern ridge of the catchment and a 16 m deep drill core (DC2) near the outlet of the valley floor provided unaltered parent materials free of ankerite (Jin et al., 2010). Methods of sample collection have been described in detail in previous publications; in fact the analyses reported here were completed on the same samples reported previously (e.g., Jin et al., 2010, 2011a,b; Ma et al., 2010, 2011a,b; West et al., 2011; Herndon et al., 2011; Yesavage et al., 2012).

Pertinent aspects of the sampling protocol are re-summarized here. Bulk soil samples were collected every ~10 cm throughout the soil profile at each site. One stream sediment sample was collected from the mouth of the catchment. Natural water samples (soil pore water and stream water) were also collected from the Shale Hills watershed (Fig. 1b). Soil pore waters were collected using suction lysimeters consisting of porous cups and PVC tubes (soil water samplers model 1900L from Soil Moisture, Inc.). "Nests" of lysimeters were installed in 2007 at 10 cm depth intervals at the three sites where the soil cores were collected (SPRT, SPMS, and SPVF; Fig. 1b). The tubes are 40 mm in outer diameter and have a 1.3 μm maximum pore size. After recovery from the lysimeters, soil water samples were not filtered further. Daily stream samples were collected with ISCO auto-samplers (Teledyne Isco, Inc.) at the

mouth of the catchment and filtered with 0.45 μm VWR Nylon filters (Fig. 1b). Water samples (60 ml) were acidified with ~0.3 ml ultrapure nitric acid and stored in pre-cleaned HDPE bottles and maintained at about 4 °C until analysis.

Solid sample preparation

Splits of soil samples were separated into four different particle size fractions including rock fragment (>2 mm), sand (63 μm–2 mm), silt (2 μm–63 μm), and clay (<2 μm) using a wet sieving and centrifuge procedure (Jackson, 1967). All particle size fractions and bulk solid samples (bedrock, sediment and soil samples) were air-dried and ground to pass through a 100-mesh sieve (<150 μm) before analysis.

Pb isotope analysis

Pb isotope analysis for bulk soil and bedrock samples was conducted at the University of Texas at El Paso (UTEP). All reagents used in this study were ultrapure grade (Aristar). About ~100 mg of sample powders were completely dissolved in Savillex® Teflon beakers with a three-step acid digestion procedure using concentrated HNO_3 + HF, concentrated $HClO_4$, and saturated H_3BO_3 + 6 M HCl. After digestion, sample solution was dried and re-dissolved in 1 ml 1 M HBr. Pb was separated and purified from matrix elements with a two-step column chemistry procedure employing HBr and HCl (Hanan and Schilling, 1989). More specifically, the sample in 1 M HBr was loaded onto a Teflon micro-column with Eichrom AG-1 × 8 (chloride form, 100–200 mesh) anion exchange resin. Following the column separation procedure with 1 M HBr and 6 M HCl, the eluted Pb solution was collected, dried, redissolved in 1 M HBr, and loaded into a second Teflon micro-column with a similar procedure for Pb purification. The column chemistry was conducted in a class-100 clean room. The purified Pb sample was re-dissolved in 0.05 M HNO_3 and was measured for Pb isotope ratios on an Nu Plasma HR Multiple Collector Inductively Coupled Plasma-Mass Spectrometer (MC-ICP-MS) at UTEP. The Pb isotopic analyses were carried out using standard-sample bracketing with SRM 981 Pb (correcting to values of Todt et al., 1996) and Tl doping (SRM 997 Tl and $^{205}Tl/^{203}Tl$ = 2.3889; White et al., 2000; Hanan et al., 2004, 2008; Konter and Jackson, 2012) to correct for instrument mass bias and drift (White et al., 2000). Measurements were conducted in static mode, consisting of 60 cycles of ratio measurements, including a correction for ^{204}Hg by monitoring ^{202}Hg.

For data quality assessment, the long-term average for standard SRM NBS 981 Pb used in this study is $^{206}Pb/^{204}Pb = 16.943 \pm 0.003$, $^{207}Pb/^{204}Pb = 15.500 \pm 0.003$, and $^{208}Pb/^{204}Pb = 36.726 \pm 0.008$ ($\pm 2\sigma$; Table 1). The reported uncertainties for each sample represent in-run precision. Procedural blanks ($n = 3$) were ~25 pg Pb, less than 0.1% of the Pb in samples; no blank corrections were included in the calculations. The Pb isotope ratios measured for the USGS rock standard BCR-2 over a period of 4 weeks were: $^{206}Pb/^{204}Pb = 18.761 \pm 0.004$, $^{207}Pb/^{204}Pb = 15.623 \pm 0.005$, $^{208}Pb/^{204}Pb = 38.723 \pm 0.032$ ($n = 4$; 2SD; Table 1), in agreement with previously reported literature values ($^{206}Pb/^{204}Pb = 18.753 \pm 0.020$, $^{207}Pb/^{204}Pb = 15.625 \pm 0.004$, $^{208}Pb/^{204}Pb = 38.724 \pm 0.041$; Weis et al., 2006).

Pb, Cd, and Zn concentration measurements

For Pb, Cd, and Zn concentration analysis, about 100 mg of powdered samples (bulk soil, size fractions, sediment, and bedrock) were digested using a similar acid digestion procedure as above. Pb, Cd, and Zn concentrations were determined on diluted sample solutions on an ICP-MS (Thermo Fisher Scientific XS 2) at The Pennsylvania State University. The Pb, Cd, and Zn concentrations were calibrated with a series of elemental standards, prepared from NIST traceable High Purity Standards. Analytical precision for Pb, Cd, and Zn are better than 3%. Pb, Cd, and Zn concentrations were also measured for USGS BCR-1, RGM-1, AGV-1, and NIST 1643e standards. The measured Pb, Zn, and Cd concentrations are in agreement with standard reference values with accuracy better than 5%, 2% and 4%, respectively (Table 2).

For water samples, dissolved Pb concentrations were also measured with the ICP-MS at Pennsylvania State University. For

Table 1
Pb isotope ratios in bulk soils and bedrock samples from Shale Hills.

Sample name	Depth (cm)	$^{206}Pb/^{204}Pb$	±	$^{207}Pb/^{204}Pb$	±	$^{208}Pb/^{204}Pb$	±
Soils							
SPRT 0010	5	19.218	0.003	15.679	0.003	39.139	0.008
SPRT 1020	15	19.606	0.003	15.700	0.003	39.640	0.008
SPRT 2030	25	19.924	0.003	15.710	0.003	40.076	0.008
SPMS 0010	5	19.436	0.003	15.696	0.003	39.391	0.008
SPMS 1020	15	19.702	0.003	15.710	0.003	39.738	0.008
SPMS 2030	25	19.856	0.003	15.692	0.003	39.926	0.008
SPMS 3040	35	19.840	0.003	15.717	0.003	39.862	0.008
SPMS 4050	45	20.018	0.003	15.722	0.003	40.205	0.008
SPMS 5059	54.5	20.228	0.003	15.737	0.003	40.484	0.008
SPVF 0010	5	19.224	0.003	15.680	0.003	39.038	0.008
SPVF 1020	15	19.799	0.003	15.718	0.003	39.854	0.008
SPVF 2030	25	20.344	0.003	15.752	0.003	40.491	0.008
SPVF 3040	35	20.006	0.003	15.726	0.003	40.163	0.008
SPVF 4050	45	20.126	0.003	15.741	0.003	40.306	0.008
SPVF 5060	55	20.341	0.003	15.743	0.003	40.650	0.008
SPVF 6067	63.5	20.342	0.003	15.746	0.003	40.706	0.008
Bedrock							
DC1-8	100	21.097	0.003	15.794	0.003	41.878	0.008
DC1-26	600	20.971	0.003	15.787	0.003	41.716	0.008
Pb isotope standards							
BCR-2 ($N = 4$)		18.768	0.004	15.633	0.005	38.749	0.032
NBS 981 (long term average)		16.943	0.003	15.499	0.003	36.727	0.008

The first four letters refer to the site (south planar ridge top, mid slope, or valley floor) and the subsequent four numbers give the depth interval of the sample in centimeters (e.g. 0010 indicates 0–10 cm, etc.). DC1 is a core from a borehole on the northern ridge of the watershed (see Jin et al., 2010) and DC2 is a core from the valley floor of the watershed (see Brantley et al., 2013). N = number of replicates.

Table 2
Pb, Cd, Zn, and Zr concentrations in bulk soil, particle size fraction, sediment, and bedrock samples from Shale Hills.

Sample name	Depth (cm)	Pb in bulk soil (mg/kg)	Pb in particle size fractions				Zn in bulk soil (mg/kg)	Cd in bulk soil (mg/kg)	Zr (mg/kg)[a]
			>2 mm (mg/kg)	Sand (mg/kg)	Silt (mg/kg)	Clay (mg/kg)			
Soils									
SPRT 0010	5	30.3	13.7	27.0	66.3	140.0		0.29	249
SPRT 1020	15	12.7	12.5	35.7	34.2	75.2	92.3	0.14	275
SPRT 2030	25	20.6	9.8	21.5	28.3	76.2		0.09	246
SPMS 0010	5	17.8	15.9	35.4	40.3	104.0	77.3	0.17	351
SPMS 1020	15	11.5	13.0	27.7	33.8	107.3	68.7	0.09	329
SPMS 2030	25	9.3	12.5	15.8	32.5	94.2	70.4	0.09	295
SPMS 3040	35		10.0	26.7	42.8	108.8			288
SPMS 4050	45	8.3	10.2	15.5	35.9	98.5	70.4	0.10	277
SPMS 5059	54.5	6.7	7.2	18.8	47.9	122.5	67.4	0.10	266
SPVF 0010	5	32.6						0.28	349
SPVF 1020	15	11.1	15.9	22.2	21.8	48.9	68.7	0.10	318
SPVF 2030	25	6.9	7.5	16.7	25.8	62.7	69.9	0.09	258
SPVF 3040	35	8.4	7.8	14.6	22.3	42.9	78.7	0.09	219
SPVF 4050	45	7.7	6.0	30.9	18.0	26.5	74.0	0.09	208
SPVF 5060	55	6.7	7.9	9.1	17.7	25.3	72.4	0.08	182
SPVF 6067	63.5	13.5	7.2	8.9	15.5	24.2		0.12	191
Sediment		16.3					96.0	0.40	
Bedrock									
DC1-8	100	5.7					74.1	0.08	
DC1-36	2100	4.3						0.05	
DC1-38	2200	4.8					91.7	0.10	
DC2-1718	534	3.4					60.8	0.05	
DC2-2223	686	5.9					74.7	0.12	
DC2-5152	1570	3.5					77.2	0.04	
Bedrock average		*4.6*					*75.7*	*0.1*	*178*
Standards									
BCR1		11.37							
Reference		11 ± 2							
NIST1643e		19.11						6.63	
Reference		*19.15 ± 0.20*						*6.41 ± 0.07*	
AGV-1		34.33					89.6		
Reference		*36 ± 5*					*88 ± 9*		
RGM-1		23.55					32.16		
Reference		*24 ± 3*					*32 ± 3*		

[a] Zr concentrations from Jin et al. (2010).
[b] Reference values for standards are from USGS and NIST websites.

this study, 12 soil pore waters and 7 stream waters, collected from the stream outlet in November 2009, were selected for Pb concentration measurements. Analytical precision for Pb is better than 3%.

Results

Pb isotope ratios in bulk soil and bedrock are listed in Table 1. Pb, Cd, and Zn concentrations in bulk soil, stream sediment, and bedrock, as well as Pb concentrations in four particle size fractions in soils are listed in Table 2. All of the bulk soil samples were previously measured for concentrations of major elements (including Mg, Al, Fe, and Si) and trace elements (REE and Zr), cation exchange capacity (CEC), loss on ignition (LOI), organic matter content, and mineralogical composition (Jin et al., 2010; Andrews et al., 2011). Zr concentrations are included in Table 2 for reference. Pb concentrations in soil pore water and stream water are listed in Table 3.

Pb concentrations in the bedrock samples range from 3.4 to 5.7 mg/kg (or ppm). Pb concentrations in the bulk soils and sediment range from 6.7 to 32.6 ppm, higher than the bedrock values. All three soil profiles show bulk Pb concentrations that generally increase toward the surface (Fig. 2). Zn and Cd

Table 3
Pb concentrations in soil pore water and stream water at Shale Hills (collected in November 2009).

Sample	Depth (cm)	Pb ($\mu g L^{-1}$)
Soil pore water		
SPRT	10	0.15
SPRT	20	0.06
SPRT	30	0.09
SPMS	10	0.52
SPMS	20	1.69
SPMS	40	0.05
SPMS	50	0.21
SPVF	10	0.08
SPVF	20	0.19
SPVF	30	0.11
SPVF	40	0.12
SPVF	60	0.12
Stream water		
Stream112009		0.03
Stream112109		0.06
Stream112209		0.04
Stream112309		0.04
Stream112409		0.04
Stream112509		0.05
Stream112609		0.04

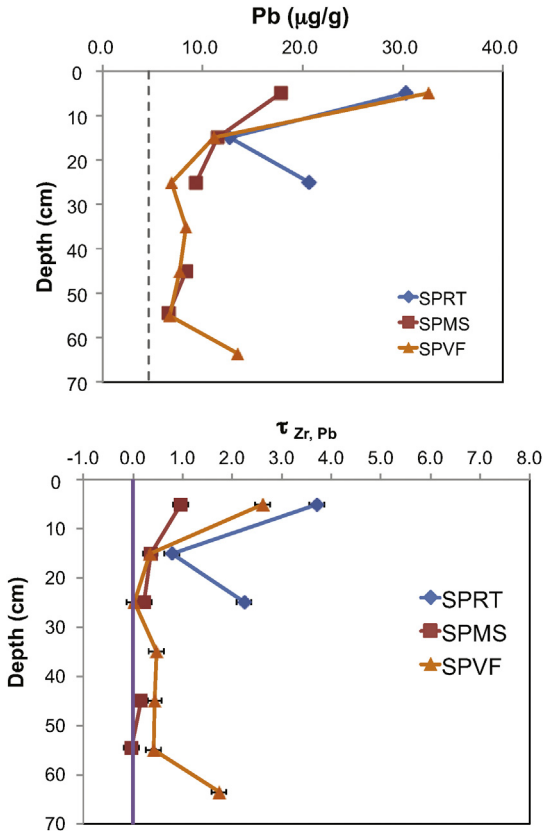

Fig. 2. (a) Pb concentrations as a function of depth in bulk soils at Shale Hills; dashed line indicates average bedrock Pb concentration, (b) Pb mass transfer coefficient ($\tau_{Zr,Pb}$) in bulk soils as a function of depth at Shale Hills. The uncertainty of Pb mass transfer coefficient is estimated to be ±0.15 considering the uncertainties of Pb concentrations in parent material and soils (see text for details).

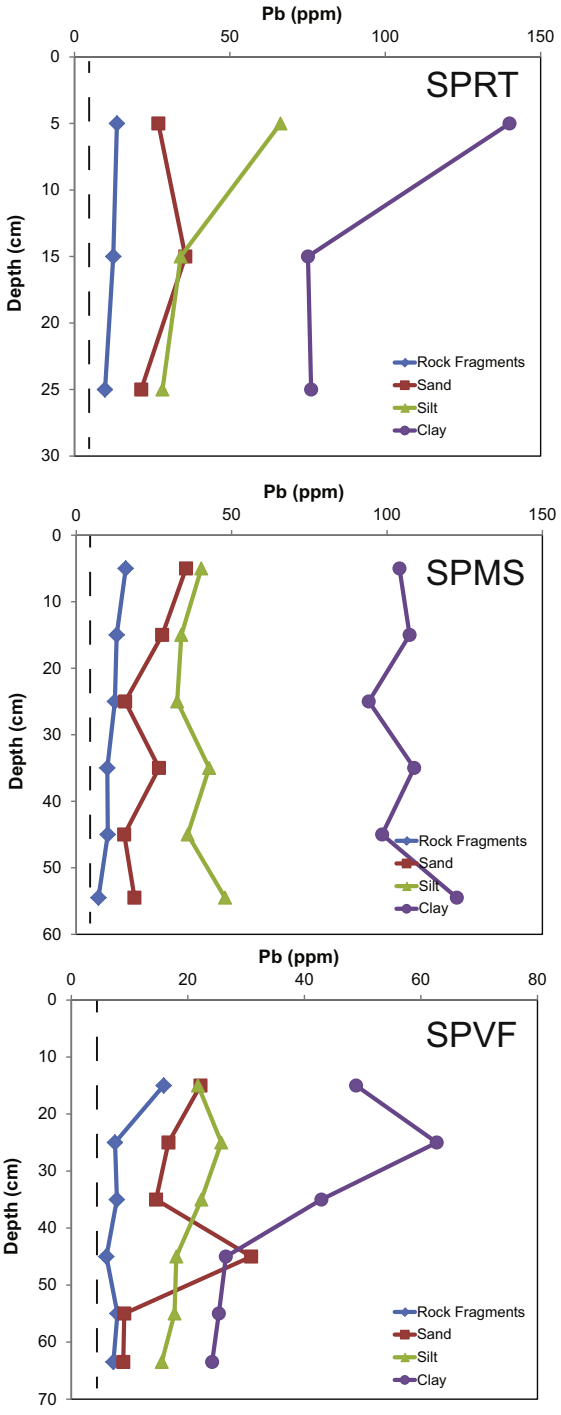

Fig. 3. Measured Pb concentrations in four particle size fractions as a function of depth at SPRT (A), SPMS (B) and SPVF (C) of Shale Hills. Dashed line indicates the average Pb concentration in bedrock for comparison.

concentrations in bulk soil samples are also higher than the bedrock values, similarly increasing toward the surface (Table 2).

Pb concentrations in the four particle size fractions generally decrease with increasing particle size from the clay fraction (24.2–140.0 ppm), to silt (15.5–66.3 ppm), to sand (8.9–35.7 ppm), and finally, to rock fragments (6.0–15.9 ppm) (Fig. 3). Notably, the Pb concentrations measured in rock fragments from the soil profiles are greater than the bedrock values. Pb concentrations in soil pore waters and stream waters range from 0.03 to 1.7 μg/kg (or ppb) (Table 2).

The Pb isotope ratios of the three soil profiles systematically decrease upward (Fig. 4). The Pb isotope ratios of surface soils (0–10 cm depth) show that $^{206}Pb/^{204}Pb$ ranges from 19.211 to 19.429, $^{207}Pb/^{204}Pb$ from 15.669 to 15.670, and $^{208}Pb/^{204}Pb$ from 39.012 to 39.365. All of these isotopic values are significantly lower than those measured for the two bedrock samples (Fig. 4 and Table 1).

Discussion

Pb addition and retention in Shale Hills soils

At least two reasons can be invoked to explain why metal concentrations increase upward in soils: (i) loss of other elements that leave the metal behind and concentrate it as weathering progresses; (ii) metals can be added to the land surface from an exogenous source.

To test for (i), i.e., to correct for relative changes in Pb concentrations due to mobility of other elements in the soils, we calculated Pb "mass transfer coefficients" ($\tau_{Zr,Pb}$) using Eq. (1) (Brimhall and Dietrich, 1987; Anderson et al., 2002):

$$\tau_{Zr,Pb} = \frac{C_{Pb,w}}{C_{Pb,p}} \frac{C_{Zr,p}}{C_{Zr,w}} - 1 \quad (1)$$

This calculation uses an immobile element (e.g. Zr) to normalize concentrations. Here, positive $\tau_{Zr,Pb}$ values indicate enrichment of Pb, negative values indicate depletion, and zero indicates no gain nor loss of Pb in the weathered soils (w) with respect to the parent

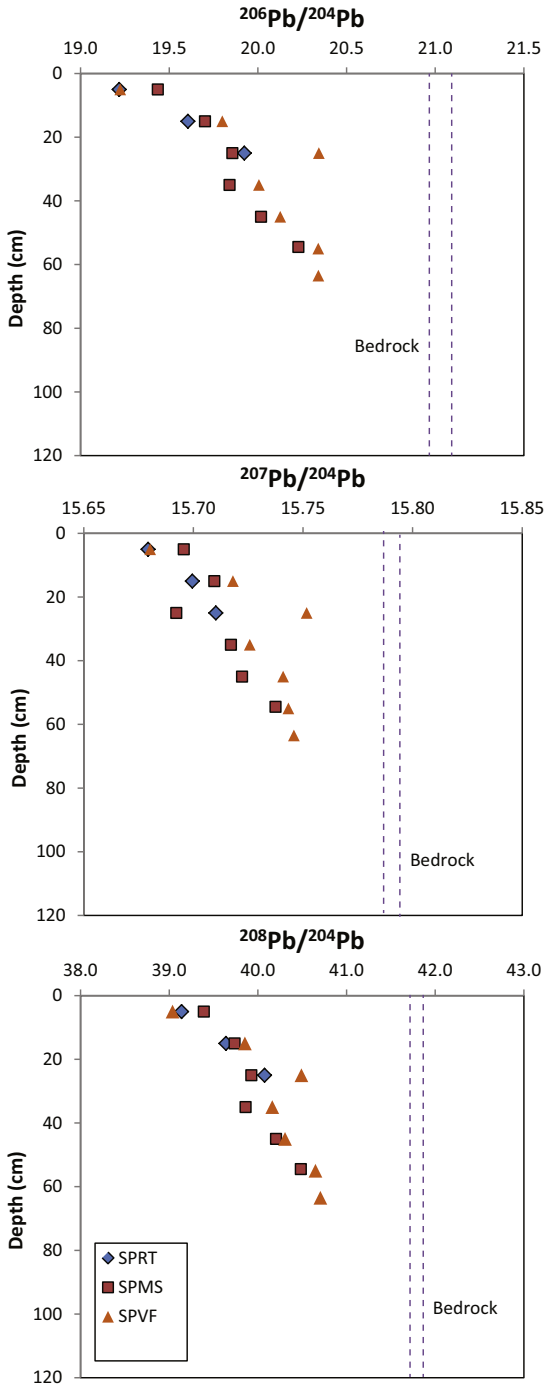

Fig. 4. Pb isotope composition in bulk soils as a function of depth at Shale Hills. Values measured in two bedrock samples (from 1 m to 6 m depth) are shown as vertical dashed lines for comparison.

material (p). C_{Zr} and C_{Pb} refer to concentrations of Zr and Pb, respectively (Table 4). Zr is used here as the reference element because of its documented immobile behavior during chemical weathering at Shale Hills (Jin et al., 2010). For positive τ values that indicate net addition to a soil, the so-called mass transfer coefficients can be considered as relative enrichment factors.

Typically, in calculating τ values for a soil profile, the largest source of error is the assumption of parent composition. This is problematic especially for sedimentary rocks such as shale because sedimentary layers may vary with lateral position and depth. However, Pb concentrations in six bedrock samples from 1 to 22 m depth (Table 1) only vary within a narrow range (4.6 ± 1.1 ppm), indicating a relatively homogenous parent material at Shale Hills with respect to Pb content. Hence, we used the average Pb concentration (4.6 ppm) in bedrock samples as the parent value (Table 4). The only other choice we considered as parent was the rock fragments within the soils themselves. Indeed, Jin et al. (2010) observed that these rock fragments have similar major element compositions to the unweathered parent bedrock. However, Pb concentrations in rock fragments recovered from the soil profiles (at 5–67 cm depth) range from 6.0 to 15.9 ppm (higher than bedrock; Table 1), and show a slight tendency to increase upward (Fig. 3). The higher Pb concentrations are consistent with the interpretation that rock fragments inside the soil profiles have been altered with respect to Pb compared to the parent bedrock.

Pb is known to have low chemical mobility during soil formation and chemical weathering (Gaillardet et al., 2004; FOREGS, 2010). If Pb were enriched at the surface only because of loss of other mobile elements such as Mg (mechanism i), $\tau_{Zr,Pb}$ would equal 0 at all depths, and this profile would be characterized as an immobile profile (Brantley and White, 2009). In contrast, Pb mass transfer coefficients ($\tau_{Zr,Pb}$) for the bulk soils in the SPRT, SPMS and SPVF profiles are mostly all positive and increase toward the surface (Fig. 2b). Indeed, the surface soils from 0 to 10 cm depth have higher $\tau_{Zr,Pb}$ values (0.96–3.71), consistent with Pb enrichments of 96–371% compared to the parent material. These profiles thus are characterized as addition profiles (Brantley and White, 2009). Addition profiles mean that, on net, Pb has been added to the soil (mechanism ii). For a ridge topsoil, addition cannot come from transport from upslope and the likely source must therefore be atmospheric or anthropogenic addition.

If $\tau_{Zr,Pb}$ values are consistently positive throughout a soil, as demonstrated in Fig. 2, then Pb must have been added to the soil from elsewhere. However, in addition, it is well known that metals can also be taken up by plants and released back to topsoil as the plants die and decompose, concentrating metals at the land surface. If plants took up Pb from depth and then re-released it to the topsoil upon decomposition, without additional Pb added to the system, then Pb depletion ($\tau_{Zr,Pb} < 0$) should be observed at the rooting depth (i.e. the depth where vegetation derived water and Pb). Such a profile – one that is depleted in an element at depth and enriched at the surface – is called a biogenic profile (Brantley and White, 2009). The profiles in Fig. 2 are not biogenic profiles, however, because the deep soil samples (e.g. 20–70 cm depth) in SPRT and SPVF show $\tau_{Zr,Pb} > 0$. Specifically, $\tau_{Zr,Pb} > 0$ even in the depth interval from which roots extract water: based on O and H isotopic measurements of tree material in the catchment, the trees extract water from the augerable soil zone (Gaines et al., 2013).

In fact, instead of Pb depletion at depth, Fig. 2 documents some evidence for Pb addition (i.e. $\tau_{Zr,Pb} > 0$) in the deep soils. This is attributed to redistribution of Pb within the soil column. Mobility after deposition could be explained by chemical dissolution and adsorption/reprecipitation at depth, especially given the surface acidic soil waters (pH ~ 3–5; Andrews et al., 2011). In addition, Pb deposited on the soil surface likely mixes downward in the soil column over time due to physical mixing (e.g., freeze–thaw), bioturbation, and adsorption/desorption (e.g., He and Walling, 1997; Kaste et al., 2007; Drivas et al., 2011).

Even given the redistribution processes, majority of the Pb is still retained in the clay-rich soils when the total Pb is considered over the entire profile. Indeed, the clay particles at Shale Hills have the highest Pb concentrations, consistent with sorption to surfaces as the likely explanation for the retention of Pb in the soil (Fig. 3). Studies of Pb dynamics in forested soils in Ontario (Canada) and Vermont (USA) also show that Pb strongly bonds to organic matter and iron oxides – both of which commonly coat clay particles (Kaste et al., 2003; Watmough et al., 2004). The Shale Hills soils

Table 4
Pb total inventory, mass transfer coefficient, Pb pollutant percentage, and Pb pollutant inventory for soil profiles at Shale Hills.

Depth range (cm)	Pb ($\mu g\,g^{-1}$)	Zr ($\mu g\,g^{-1}$)	$\tau_{Zr,Pb}$	ρ ($g\,cm^{-3}$)	ε	Total $M_{Pb,w}$ ($\mu g\,cm^{-2}$)	Pb pollutant (%)	Pollutant $M_{Pb,w}$ ($\mu g\,cm^{-2}$)
SPRT						952.1		610 ± 99
0–10	30.3	249	3.71	1.29	−0.25		80 ± 21	
10–20	12.7	275	0.79	1.60	0.03		62 ± 16	
20–30	20.6	246	2.24	1.74	0.00		48 ± 13	
SPMS						750.6		403 ± 51
0–10	17.8	351	0.96	1.09	−0.10		71 ± 18	
10–20	11.5	329	0.35	1.41	0.08		58 ± 15	
20–30	9.3	295	0.23	1.55	0.07		50 ± 13	
30–40		288		1.65	0.11		52 ± 14	
40–50	8.3	277	0.16	1.72	0.11		44 ± 12	
50–59	6.7	266	−0.03	1.77	0.10		34 ± 10	
SPVF						1149.0		583 ± 81
0–10	32.6	349	2.61	1.06	−0.14		80 ± 21	
10–20	11.1	318	0.35	1.37	0.02		54 ± 14	
20–30	6.9	258	0.03	1.52	−0.08		30 ± 9	
30–40	8.4	219	0.48	1.61	−0.17		44 ± 12	
40–50	7.7	208	0.43	1.68	−0.18		40 ± 11	
50–60	6.7	182	0.42	1.74	−0.26		29 ± 9	
60–67	13.5	191	1.74	1.78	−0.20		29 ± 9	
Average bedrock	4.6	178	0	2.4	0			

See Eqs. (1) and (2) and text in 'Pb isotope mass balance model' section for details.

contain high concentrations of Fe oxides and organic matter (Jin et al., 2010) and thus favor retention of Pb in soils.

External sources of Pb at Shale Hills

Mn enrichment has been observed in these same soils and attributed to the enhanced heavy metal emission from (1) iron production in this region from the early 19th century, (2) modern steel or coal-burning power plants nearby or to the immediate west, and (3) the combustion of Mn-enriched gasoline; Mn was added to gasoline after the use of Pb was prohibited (Herndon et al., 2011). These sources could similarly be responsible for the Pb addition profiles. Here, we compare the measured Pb isotope ratios in Shale Hills to common anthropogenic Pb isotope signatures in the United States (Fig. 5), which include (1) the use of Pb in gasoline additives in the United States and European countries from 1940s to 1990s; (2) coal burning; and (3) emission from Pb production from ore deposits (e.g., Edgington and Robbins, 1976; Graney et al., 1995; Marcantonio et al., 2002; Reuer and Weiss, 2002; Klaminder et al., 2003; Roux et al., 2005; Lima et al., 2005; Hissler et al., 2008; Geagea et al., 2008; Kelly et al., 2009).

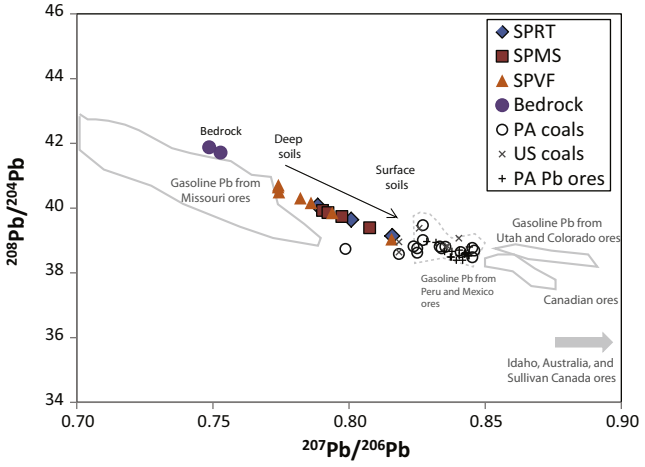

Fig. 5. Comparison of Pb isotopic composition ($^{208}Pb/^{204}Pb$ vs. $^{207}Pb/^{206}Pb$) in Shale Hills samples to common sources of Pb used in the United State. Coal and Pb ore samples from Pennsylvania are shown in open circles and plus symbols, respectively. Isotopic signatures of the major sources of gasoline Pb in this region are from Missouri, Idaho, British Columbia and Australia (Graney et al., 1995) are shown as gray outlined areas. Dashed gray lines show the values for Pb ores from Mexico and Peru, which were not used as gasoline additives in the Great Lakes region (Graney et al., 1995).
Data sources are Chow and Earl (1972), Andrews et al. (1984), Cumming and Richards (1975), Cumming et al. (1979), Doe and Delevaux (1972), Gulson et al. (1981), Gunnesch et al. (1990), Heyl et al. (1974), Thompson and Beaty (1990) and Graney et al. (1995).

The Shale Hills soils define an isotopic trend with depth: deeper soil samples plot closer to the bedrock sample while shallower soil samples plot further away. Although both domestic and imported Pb ores were used in gasoline production in United States from 1940 to 1990 (e.g., Graney et al., 1995), the most common gasoline Pb source was ore from Missouri (Mississippi Valley type ore deposits). Indeed, reconstructed Pb isotope records using lake sediments in the Great Lakes region have documented that the gasoline-related emissions that were deposited in that region derived mainly from Pb ores from Missouri, Idaho, British Columbia and Australia (Graney et al., 1995). However, surface soil samples at Shale Hills have Pb isotope signatures that are distinct from these gasoline Pb sources and similar to the Pennsylvanian coals and Pb ore deposits (Fig. 5).

The simplest explanation for these observations is that the added Pb in Shale Hills derived from utilization of local coals or Pb ores. For instance, iron furnaces and forges were widely used in Pennsylvania up until the 1920s (Fig. 1). Iron production started in Pennsylvania as early as 1716 and grew rapidly (e.g., Eggert, 1994). By 1850 when iron production from this area probably was at its maximum, 48 furnaces and 42 forges were operating in the "Juniata Iron Region" consisting of Blair, Centre, Clinton, Huntingdon, and Mifflin Counties (Fig. 1). This region produced more iron than any single U.S. county in the late 1800s (Eggert, 1994): by the 1850s, most of these Pennsylvania (PA) iron furnaces were located in central and western PA (Fig. 1). The PA iron was used to build tools, locomotives, and iron rails for the U.S.A. in the 18th and 19th centuries. The primary fuel for the iron-blasting furnaces after the 1850s was "coke", a product produced by heating local (Pennsylvania) coal. The continued rise in demand for iron and steel drove an increase in coal production (and by implication, burning) of 300% from 1850 to early 1880s (Eggert, 1994). By the

early 1900s, coal was supplying more than 100,000 ovens to make coke, mostly in western Pennsylvania and northwestern West Virginia (Eggert, 1994).

Shale Hills is located at the center of the "Juniata Iron Region" (Fig. 1). Indeed, several large iron furnaces in central Pennsylvania were operating only ~10 km away from the Shale Hills. Ruins of the Monroe furnace is found ~3 km from the watershed. In total, there were 29 major iron furnaces operating in Huntingdon and neighboring Blair counties until the early 20th century. Shale Hills is also downwind of both the concentrations of iron furnaces and coal plants in western PA because the dominant wind direction in the area is from west to east (Lima et al., 2005). In addition to coal burning, Pb smelting activities were also active in regions west of Shale Hills during the early industrial revolution (e.g. galena ores from Fort Roberdeau were used in local smelters near Tyrone, PA). Hence, it is reasonable to argue that based on the Pb isotope ratios, the external Pb source that delivered Pb to the Shale Hills soil is not related to the use of leaded gasoline from 1940s to 1990s in the United States, but rather the local metal production during the early industrial revolution such as coal burning and iron/Pb ore smelting.

Pb deposition rates into Shale Hills

Below, we use two independent models to quantify the Pb deposition rates into Shale Hills during the iron production period from 1850 to 1920. The first model, Pb isotope mass balance model ('Pb isotope mass balance model' section), uses Pb isotope ratios to determine anthropogenic Pb inventory in soil profiles and atmospheric deposition rates. The second model, Pb mass flux box model, determines Pb deposition rates by simulating the change of total Pb inventory with time with Pb input and output fluxes of a soil profile.

Pb isotope mass balance model

The mass of Pb in soil per unit land surface area for one depth interval Δz (cm) is $\Delta z \rho_w C_{Pb,w}$. Here ρ_w is the average bulk density (g cm^{-3}) of the soil sample for Δz. This value is estimated from our previously determined relationship between soil density and depth at Shale Hills (Ma et al., 2013; Table 4). $C_{Pb,w}$ is Pb concentration in bulk soils (mg/kg). The total Pb inventory $M_{Pb,w}$ (μg cm^{-2}) in soil integrated over the entire augerable profile is thus $M_{Pb,w} = \sum(\Delta z \rho_w C_{Pb,w})$, where the summation is performed over all depth intervals that contain Pb. The values for the total Pb inventories ($M_{Pb,w}$) calculated for SPRT, SPMS and SPVF profiles are 950, 750, and 1150 μg cm^{-2}, respectively (Table 4). The total Pb inventory ($M_{Pb,w}$) includes Pb derived both from the bedrock by chemical weathering and from exogenous sources. The percentage of Pb added to the soil – here assumed to be from an anthropogenic source, i.e., $Pb_{anthropogenic}$ (%) – can be estimated by using measured Pb isotope ratios in a soil sample ($^{207}Pb/^{206}Pb_{sample}$) along with isotope ratios of the exogenous source ($^{207}Pb/^{206}Pb_{anthropogenic}$) and the bedrock ($^{207}Pb/^{206}Pb_{natural}$). We follow other researchers (Reuer and Weiss, 2002) by using $^{207}Pb/^{206}Pb$ ratios in Eq. (2):

$$Pb_{anthropogenic} = \left[1 - \frac{^{207}Pb/^{206}Pb_{sample} - {}^{207}Pb/^{206}Pb_{anthropogenic}}{^{207}Pb/^{206}Pb_{natural} - {}^{207}Pb/^{206}Pb_{anthropogenic}}\right] \times 100\% \quad (2)$$

Here, we used the average measured bedrock value ($^{207}Pb/^{206}Pb = 0.751 \pm 0.003$) as $Pb_{natural}$ and the average Pennsylvania coal value ($^{207}Pb/^{206}Pb = 0.83 \pm 0.01$; Chow and Earl, 1972) as $Pb_{anthropogenic}$. Another possible Pb source is Pennsylvania Pb ores that have similar Pb isotope composition as PA coals (Fig. 5). The calculated anthropogenic Pb contribution ranges from 29 ± 9 to 80 ± 21% for the three profiles at Shale Hills (Table 4), with higher percentages observed in soils at shallow depths and toward the ridge top. Despite the fact that Pb concentrations (which range up to 33 ppm) in soils at Shale Hills are not extremely high as compared to values reported for heavily contaminated topsoils in industrial and urban settings (e.g. ~970 ppm in European soils; FOREGS, 2010), the high percentages of anthropogenic Pb (up to 80%) reveal that the Pb mass balance has nonetheless been dominated by anthropogenic sources.

Integrated over the entire profile, anthropogenic sources thus contributed 610 ± 100, 400 ± 50, and 580 ± 80 μg Pb cm^{-2} in SPRT, SPMS and SPVF profiles, respectively (Table 3). If the anthropogenic Pb was added to the topsoils only during the iron production period from 1850 to 1920, this would lead to average atmospheric Pb deposition rates at Shale Hills of $\sim 6 \pm 1$ to 9 ± 1 μg cm^{-2} yr^{-1}. Alternatively if we consider the Pb emission from coal-burning activities in Pennsylvania as a continuous process from 1850 to today, the atmospheric Pb deposition rates at Shale Hills would be $\sim 3 \pm 1$ to 4 ± 1 μg cm^{-2} yr^{-1}. Either of these values would most likely represent minimum *net* atmospheric Pb deposition rates, i.e., net deposition after chemical leaching of Pb.

Pb mass flux box model

We also estimate rates of atmospheric Pb deposition to Shale Hills soils with a Pb mass flux model. This model considers input (bedrock weathering and anthropogenic deposition) and output (chemical weathering and physical erosion) mass fluxes to a soil profile using the measured Pb concentrations in soils and water as well as soil production and erosion rates. This Pb box model approach is modified from Herndon et al. (2011), where it was used to estimate the atmospheric Mn deposition rates for Shale Hills.

For this calculation, we only consider the ridge top site, where no sediment has been transported and deposited from upslope positions. The input flux of Pb to the SPRT profile from bedrock weathering (B) can be calculated as $B = C_{Pb,p}\rho_p\omega = 0.05$ μg cm^{-2} yr^{-1}. Here $C_{Pb,p}$ is the Pb concentration in bedrock (4.6 μg g^{-1}; Table 5), ρ_p is the bedrock density (2.4 g cm^{-3}; Jin et al., 2010), and ω is the soil production rate (0.0045 cm yr^{-1}; determined from U-series isotope disequilibrium by Ma et al., 2010).

The output flux of Pb from soils due to chemical weathering, W (0.0054 μg cm^{-2} yr^{-1}), is calculated as $W = (MAP - ET)C_{Pb,water}\rho_{water}$. Here MAP is the mean annual precipitation (107 cm yr^{-1}; NOAA, 2007), ET is the water loss due to evapotranspiration (~53 cm yr^{-1}; Jin et al., 2011a,b), and $C_{Pb,water}$ is the average Pb concentration in soil pore water, estimated from the measured Pb concentrations in the SPRT pore water (0.0001 μg g^{-1}; Table 5). ρ_{water} is the density of water (1 g cm^{-3}).

The output flux of Pb due to physical erosion from the surface soil (E, μg cm^{-2} yr^{-1}) can be calculated using $E = C_{Pb,w}\rho_w\varepsilon$. Here $C_{Pb,w}$ is the Pb concentration in soil (μg g^{-1}), ρ_w is the soil density (g cm^{-3}), and ε is soil erosion rate (cm yr^{-1}). Both the Pb concentrations and soil density vary with depth. To simplify the calculation, we assume a uniform Pb concentration in soils with depth ($M_{Pb,w}(t)/L$). Here L is soil thickness ($L = 30$ cm) and $M_{Pb,w}(t)$ is the total Pb inventory for SPRT at time t. Assuming a surface erosion rate ($\varepsilon \equiv 0.0045$ cm yr^{-1}) equal to the soil production rate for SPRT (following the conclusions of West et al. (2013) for this site), the value of $E(t)$ (output flux of Pb by physical erosion at a given time, t) is thus equivalent to $E(t) = \varepsilon M_{Pb,w}(t)/L$. We assume formation of soil is isovolumetric at Shale Hills. Indeed, the volume strain calculated at Shale Hills has shown that, although the regolith has expanded, the variation in strain is less than 18% within the profile; only in the upper 3 cm layer has volume expanded significantly due to addition of organic matter (Jin et al., 2010).

Table 5
Parameters in the Pb mass balance box model.

Soil profile	$M_{Pb,w}$ ($\mu g\,cm^{-2}$)	L (cm)	B ($\mu g\,cm^{-2}\,yr^{-1}$)	$C_{Pb,p}$ ($\mu g\,g^{-1}$)	ρ_p ($g\,cm^{-3}$)	ω ($cm\,yr^{-1}$)	W ($\mu g\,cm^{-2}\,yr^{-1}$)	MAP ($cm\,yr^{-1}$)	ET ($cm\,yr^{-1}$)	$C_{Pb,water}$ ($\mu g\,g^{-1}$)	ε ($cm\,yr^{-1}$)	A_{70yrs} ($\mu g\,cm^{-2}\,yr^{-1}$)	A_{160yrs} ($\mu g\,cm^{-2}\,yr^{-1}$)
SPRT	1100	30	0.093	8.6	2.4	0.0045	0.0054	107	53.5	0.0001	0.0045	10	4

For a given anthropogenic input, A ($\mu g\,cm^{-2}\,yr^{-1}$), the total Pb inventory in a soil profile ($M_{Pb,w}$) from time t to $t+1$ can be calculated as:

$$M_{Pb,w}(t+1) = M_{Pb,w}(t) + A + B - W - E$$
$$= M_{Pb,w}(t) + A + B - W - \frac{\epsilon M_{Pb,w}(t)}{L} \quad (3)$$

Under natural conditions when the anthropogenic Pb deposition is negligible ($A = 0\ \mu g\,cm^{-2}\,yr^{-1}$), the total Pb inventory in SPRT calculated from Eq. (3) increases from the initial condition ($M_{Pb,w} = 0\ \mu g\,cm^{-2}$ when $t = 0$) to a steady state value of $\sim$280 $\mu g\,cm^{-2}$ in about 20,000 years (blue line in Fig. 6). In other words, this is the steady-state Pb inventory due to Pb inputs from bedrock alone. Given that the soil residence time for SPRT determined by U-series isotopes and ^{10}Be inventory is $\sim$7000–9000 years (Ma et al., 2013); it is likely the total Pb inventory in SPRT should have been close to the steady state value ($\sim$280 $\mu g\,cm^{-2}$) in the absence of anthropogenic Pb. However, the measured total Pb inventory in SPRT (950 $\mu g\,cm^{-2}$) is significantly greater (Fig. 6), consistent with the conclusion that the SPRT profile has recently received anthropogenic Pb deposition.

In order to increase the Pb inventory from 280 to 950 $\mu g\,cm^{-2}$ in 70 years (i.e. from 1850 to 1920), our model simulation requires an anthropogenic Pb deposition rate of 10 $\mu g\,cm^{-2}\,yr^{-1}$ (A_{70yrs} in Fig. 6). If the time period in consideration is $\sim$160 years (i.e. from 1850 to 2010), the required anthropogenic Pb deposition rate on average is then 4 $\mu g\,cm^{-2}\,yr^{-1}$ (A_{160yrs} in Fig. 6). Once again, this model only strictly applies to ridge top sites where no lateral transport adds Pb as solute or sediment.

Comparison to other Pb deposition rates

Both Pb mass balance models yield consistent atmospheric Pb deposition rates for Shale Hills of $\sim$6–10 $\mu g\,cm^{-2}\,yr^{-1}$ if the Pb emission is mainly from 1850 to 1920 or about 3–4 $\mu g\,cm^{-2}\,yr^{-1}$ if from 1850 to 2010 (Fig. 7). These Pb deposition rates are much higher than those determined for other parts of the northeastern and Great Lake regions of the U.S.A. (Fig. 7). For example, modern wet Pb deposition rates (by rain and snow) have been determined for the time period 1990–2010 to be 0.04–0.06 $\mu g\,cm^{-2}\,yr^{-1}$ for the Chesapeake Bay region in Maryland, northern Virginia, and Delaware (Kim et al., 2000; Conko et al., 2004). Those low modern wet Pb deposition rates presumably reflect the effects of reduced

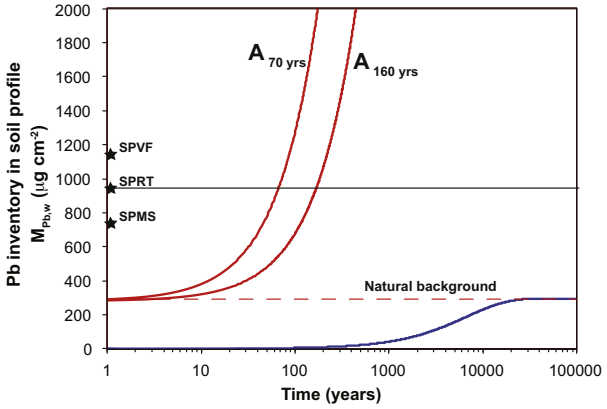

Fig. 6. Pb inventory mass balance model for SPRT site at Shale Hills. Blue line shows the calculated increase in natural Pb inventory in the soil as a function of time with $A = 0\ \mu g\,cm^{-2}\,yr^{-1}$ and initial $M_{Pb,w} = 0\ \mu g\,cm^{-2}$. Red solid lines indicate the increase of Pb inventory as a function of time with $A = 4\ \mu g\,cm^{-2}\,yr^{-1}$ and $10\ \mu g\,cm^{-2}\,yr^{-1}$, respectively and initial $M_{Pb,w} = 280\ \mu g\,cm^{-2}$. The total Pb inventory in SPRT, SPMS, and SPVF are shown for reference.

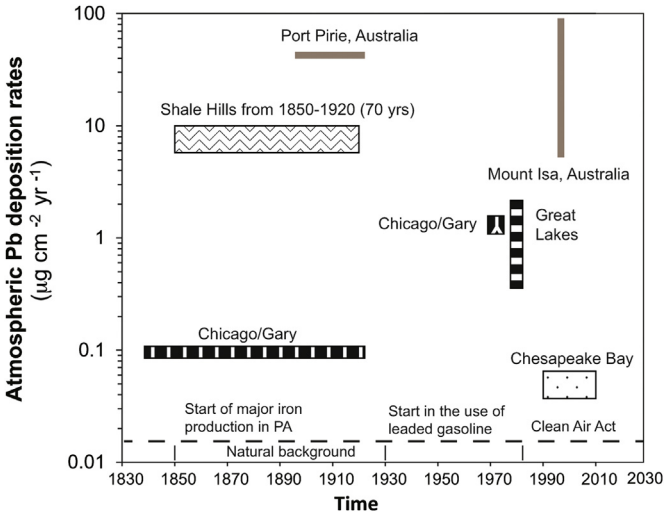

Fig. 7. Comparison of atmospheric Pb deposition rates in Shale Hills to those determined for other parts of the northeastern and Great Lake regions of the U.S.A. and historical industrial areas in Australia as described in the text (Burkitt et al., 1972; Edgington and Robbins, 1976; Eisenreich et al., 1986; Kim et al., 2000; Conko et al., 2004; Reuer and Weiss, 2002; Mackay et al., 2013). For each estimated deposition rate, the time period of deposition is indicated. Natural background Pb deposition is shown as a dashed line. Also shown for comparison as small vertical lines near the *x*-axis are the start of major iron production in PA, the initial use of Pb in gasoline, and the Clean Air Act.

Pb emissions to the atmosphere since the mandatory use of unleaded gasoline was instituted in the 1980s (the Clean Air Act; http://www.epa.gov/air/caa/).

The deposition rates we estimate at Shale Hills are also larger than those from gasoline-related deposition – which presumably peaked soon after the peak in anthropogenic Pb emission from leaded gasoline peaked in 1979 (Eisenreich et al., 1986). For example, the wet Pb deposition rates for the Great Lake region from 1970 to 1980 were estimated to be 0.4–2 $\mu g\ cm^{-2}\ yr^{-1}$ (Edgington and Robbins, 1976; Eisenreich et al., 1986). It is surprising that the Pb deposition rates calculated at Shale Hills are greater than those associated with wet deposition due to the use of leaded gasoline. After all, gasoline-derived Pb has been considered as the most dominant source of Pb pollution from the 1940s to 1990s (Nriagu and Pacyna, 1988).

However, the burning of coal and ore smelting in furnaces produces particles of relatively large size (e.g. tens of microns; Clarke and Sloss, 1992), which could only be transported in the atmosphere over a relatively short distance (e.g. tens to hundreds of kms; Reuer and Weiss, 2002). In contrast to these larger Pb particles, the emission of gasoline-derived Pb occurred as sub-micron particles that could be transported over hemispheric distances before returning to Earth's surface. Thus, those particles could be dispersed at much larger spatial scales with an "apparently low" deposition rate (Reuer and Weiss, 2002; Barrett et al., 2012). The high Pb deposition rate recorded at Shale Hills could therefore be consistent with the presence of local anthropogenic point sources upwind of the Shale Hills catchment, e.g., several iron production furnace were only located ~less than 10 km away from Shale Hills (the Monroe furnace is only ~3 km away). Furthermore, this local furnace was only one among many furnaces in central and western Pennsylvania during the industrial revolution period.

Furthermore, soils from other industrially impacted areas also show similarly high local Pb deposition rates during the early industrial revolution period. For example, in the region around Port Pirie in South Australia, at least 40,000 tons of Pb were deposited into the soils surrounding local lead smelters (2800 km^2) from 1889 to 1925, corresponding to a Pb deposition rate of ~40 $\mu g\ cm^{-2}\ yr^{-1}$ (Burkitt et al., 1972). High Pb deposition rates have also been found in modern mining and smelting regions such as copper and lead mining at Mount Isa in Australia (Mackay et al., 2013): lead-in-dust deposition during 2003–2007 was observed to range from 5 to 88 $\mu g\ cm^{-2}\ yr^{-1}$ within 3 km distance from the mines and smelters at Xstrata Mount Isa Mines. The Pb deposition rates found at Shale Hills are comparable to these local rates near industrially impacted regions (Fig. 7), suggesting that Shale Hills soils may lie directly within an area of high metal emission and deposition. Importantly, during the period of high emission near Shale Hills, 28 other iron furnaces were also operating, indicating that relatively widespread but patchy accumulation of small amounts of Pb in Pennsylvania soils most likely occurred (Fig. 1).

These conclusions do not undermine the inference that gasoline-derived Pb has heavily impacted the environment globally, but our work does suggest that local point sources are also important for understanding metal deposition at small catchment scales. As pointed out by Herndon et al. (2011), both Pb and Mn enrichment may be common and widespread in a patchy distribution related to emitting sources. At Shale Hills, the use of local PA coal in the iron blast furnaces and Pb smelting activities in Pennsylvania from 1850 to 1920 is the likely cause of the enhanced deposition of these two metals. Such enrichments may be patchy in nature both because of the non-homogenous distribution of point sources of emission, and the small length scales of large particle transport in the atmosphere.

Moderate enrichment of Pb in surface soils at Shale Hills

Although Pb deposition rates at Shale Hills are comparable to high rates found in other industrial areas, the surface soils at Shale Hills are only moderately enriched in Pb, e.g. up to 33 ppm which is about 8 times the Pb concentrations observed in natural background. Studies for heavily contaminated topsoils in industrial and urban settings have typically documented very high concentrations of Pb up to ~970 ppm in European soils – i.e., 10–20 times natural background (FOREGS, 2010). Such a moderate enrichment of Pb in surface soils at Shale Hills is attributed to Pb redistribution into deeper soil profiles after deposition, as both Pb concentrations and isotope ratios at Shale Hills (Figs. 2 and 4) have revealed the presence of anthropogenic Pb at depth. If we assume that all the anthropogenic Pb was originally located in the surface soil layer (e.g. 0–5 cm), then the total anthropogenic Pb inventory in SPRT, SPMS, and SPVF profiles can be back-calculated to a Pb concentration of 60 ppm in surface soils. Such Pb concentrations are ~15 times higher than natural background values at Shale Hills. These enrichment factors are then similar with other industrial areas.

Timing and duration of Pb atmospheric deposition and subsequent migration

Given the evidence that the Pb is simultaneously sorbed to particle surfaces but is also redistributing within the profile, Pb deposited at the land surface likely mixes downward in the soil column over time due to physical mixing (e.g., freeze–thaw) and bioturbation (e.g., He and Walling, 1997; Kaste et al., 2007; Drivas et al., 2011). Dissolution and re-precipitation may also be occurring, although the evidence that Pb is retained in the soils may mean that little net loss occurs. The Pb downward migration in soil profiles can be modeled by an advection and diffusion-like process in which the advective transport is due to downward movement of water and soils and diffusion-like transport is due to soil mixing (He and Walling, 1997; Kaste et al., 2007; Brantley and Lebedeva, 2011). Drivas et al. (2011) have shown that for Pb that is

relatively insoluble chemically, the "diffusion-only" approximation provides a reasonably accurate and practical solution to explain profiles in a wide variety of soil types and locations. Here we use the 1D diffusive Pb transport model presented by Drivas et al. (2011) to examine the Pb soil profiles at Shale Hills and to confirm the timing of the Pb deposition event.

The governing equation for vertical Pb diffusive transport in a soil column is:

$$\frac{\partial C_{Pb}}{\partial t} = D_{eff}\frac{\partial^2 C_{Pb}}{\partial z^2} \quad (4)$$

where C_{Pb} is the Pb concentration in soils (g cm^{-3}), D_{eff} is the effective diffusion coefficient (cm^2 yr^{-1}), and z is depth (cm) and t is time (yr). The analytical solutions to Eq. (4) for a variety of boundary conditions and initial conditions have been summarized by Drivas et al. (2011). To understand how the timing and duration of Pb deposition affects a Pb profile, we consider three scenarios of Pb deposition at Shale Hills: (1) a period of continuous high Pb deposition rate (A = 10 μg cm^{-2} yr^{-1}) for 70 years (1850–1920) during iron production, followed by a 90-year deposition-free period (1920–2010); (2) a period of continuous Pb deposition (A = 10 μg cm^{-2} yr^{-1}) in the recent 70 years (from 1940 to 2010) corresponding to modern coal burning in power plants; and (3) a period of continuous Pb deposition (A = 4 μg cm^{-2} yr^{-1}) for 160 years (from 1850 to 2010), corresponding to a constant Pb emission from coal burning and other activities since the industrial revolution.

For case 1, the analytical solution (Drivas et al., 2011) is:

$$C_{Pb}(z,t) = \frac{Az}{D_{eff}}\left[\frac{\exp(-S_L^2)}{\sqrt{\pi}S_L} + \mathrm{erf}(S_L) - \frac{\exp(-S_U^2)}{\sqrt{\pi}S_U} - \mathrm{erf}(S_U)\right] \quad (5)$$

where $S_L = z/2\sqrt{D_{eff}t}$ and $S_U = z/2\sqrt{D_{eff}(t-T)}$. T is the deposition-free period (90 years) and t is the time since the deposition occurred (160 years). For cases 2 and 3, Drivas et al. present in Eq. (6):

$$C_{Pb}(z,t) = \frac{2A}{D_{eff}}\left[\sqrt{\frac{D_{eff}t}{\pi}}\exp\left(\frac{-z^2}{4D_{eff}t}\right) - \frac{z}{2}\mathrm{erfc}\left(\frac{z}{2\sqrt{D_{eff}t}}\right)\right] \quad (6)$$

For each scenario, the changes of anthropogenic Pb concentrations with time were calculated for a soil column with 60 cm depth. To directly compare with our $\tau_{Zr,Pb}$ profiles, the calculated C_{Pb} concentrations were converted to the $\tau_{Zr,Pb}$ notation using Eq. (1) using an average bulk soil density (1.8 g cm^{-3}) and Pb concentration in parent bedrock equal to 4.6 μg g^{-1}.

For a given deposition history, the shape of the modeled Pb profiles largely depends on D_{eff}: higher D_{eff} correspond to a faster downward Pb migration. In undisturbed soils, values of D_{eff} have been shown to vary from 0.5 to 2 cm^2 yr^{-1} depending on soil types and locations (Drivas et al., 2011). For the above three scenarios, we ran simulations with different values of D_{eff} between 0.5 and 2.0 (in intervals of 0.25 cm^2 yr^{-1}). For all cases, the best-fit value was 2 cm^2 yr^{-1}. Similarly high diffusive coefficients for Pb have been observed for soils in France and California (Kaste et al., 2007; Fernandez et al., 2008).

In Scenario 1 (high-early deposition) and Scenario 3 (continuous deposition), Pb migrates into the deep part of the profile with time due to mixing simulated as a diffusive process (Drivas et al., 2011). Both curves (S1 and S3 in Fig. 8) are somewhat similar to the observed $\tau_{Zr,Pb}$ values (~2–4) in the RT and VF profile. By contrast, Scenario 2 (S2: high-late deposition, gray dashed line in Fig. 8), simulating a late Pb deposition in the last 70 years, result in high Pb enrichments at the soil surface i.e., $\tau_{Zr,Pb}$ values up to 7.5 that cannot be accounted for by the observed values in soils. The deposited Pb would not yet have migrated downward as deeply as observed, even with a high value D_{eff} = 2 cm^2 yr^{-1} in Scenario 2.

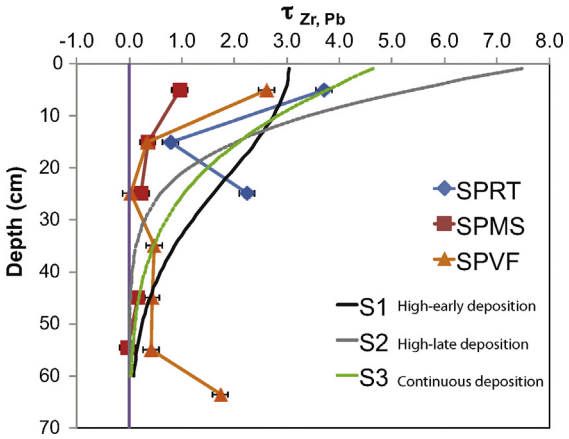

Fig. 8. Pb redistribution in soil profiles modeled by a diffusive transport model (Drivas et al., 2011). Black solid curve represents a period of continuous high Pb deposition rate (10 μg cm^{-2} yr^{-1}) for 70 years followed by a period of 90-year deposition-free time (Scenario 1); Gray dashed curve represents a period of continuous Pb deposition (10 μg cm^{-2} yr^{-1}) in the recent 70 years only (Scenario 2) and green dashed curve represents a period of continuous Pb deposition (4 μg cm^{-2} yr^{-1}) for 160 years (Scenario 3). Measured $\tau_{Zr,Pb}$ values in soils are shown for comparison.

Hence, the downward Pb migration model once again is consistent with the enhanced Pb deposition from the early industrial revolution period (~160 years ago) due to the iron production in Pennsylvania.

It is noted that the model simulation only provides an approximation to represent Pb transport process in soils as advective Pb transport has been simulated as diffusion. It is likely that Pb is transported by movement of clay size particles in advecting fluids during rain events, redistributing the Pb within the soil column. Such a process is not explicitly modeled by the diffusion model; however, Drivas et al. (2011) show many soil examples where the simple diffusion model is adequate to fit profile data.

Conclusions and implications

To understand the record of metal deposition into soils in Pennsylvania, we measured Pb concentrations and isotope ratios in parent material, soil, and sediment, as well as water in a small, pristine catchment (Shale Hills). A previous study had revealed that atmospheric deposition from anthropogenic sources has contaminated soils with Mn at Shale Hills (Herndon et al., 2011). Furthermore, that work had also demonstrated that over half of the soils surveyed in Pennsylvania and in many areas of North America and Europe are enriched in Mn, Pb and Cd. Our new results from this small catchment confirm that Pb, similar to Mn, is best characterized by an addition profile (e.g., Brantley and White, 2009) and that the Pb isotope ratios in three soil profiles all systematically change from the parent material value to a less radiogenic end-member value upward in the soil.

Based on the Pb isotope ratios, the added Pb in soils at the Shale Hills CZO was likely derived from Pennsylvania coals and or Pb ores used during the iron production period in the early 19th century in Pennsylvania. Locally, the Pb deposition rates are constrained within the range of 4–10 μg cm^{-2} yr^{-1} by mass balance models. Results from a Pb diffusive migration model are also consistent with an early deposition event during the iron production period in Pennsylvania between 1850 and 1920. These soil profiles provide documentation of the effect of the industrial revolution on soils – local, patchy accumulation of metals such as Pb and Mn near the many small metal emitters in industrial areas. Such local, patchy

contamination is likely wherever atmospheric deposition from anthropogenic sources occurred into metal-retaining soils since the 1850s.

In fact, once deposited at Earth's surface, pollutant metals such as Pb and Mn can persist in contaminated soils over considerable lengths of time, e.g. ~100–200 years. The soils at Shale Hills are known for being clay-, Fe-, and organic-rich, and thus they may represent soils that are particularly likely to retain Pb deposited from ~160 years ago. Thus, although the enforcement of strict policies such as the U.S. Clean Air Act (1970) effectively reduced metal emissions to the atmosphere a few decades ago in the U.S.A. (Fig. 7), the metals that had already been deposited into topsoils since the advent of the industrial revolution may stay in the environment for at least a few hundred years. Additional research is needed to assess the extent and the impacts of historical metal deposition on soil geochemistry and ecological processes.

Acknowledgements

We would like to thank A. Chin and M. Taylor for editorial handling and comments, and M. Engle for discussions. Constructive and insightful reviews from four anonymous reviewers are also acknowledged. This work was facilitated by NSF Critical Zone Observatory program grants to CJD (EAR 07-25019) and SLB (EAR 12-39285, EAR 13-31726). This research was conducted in Penn State's Stone Valley Forest, which is supported and managed by the Penn State's Forestland Management Office in the College of Agricultural Sciences. Analytical support to LM from CEEIR at UTEP is acknowledged. Student support to DS from UTEP COURI is also acknowledged.

References

Anderson, S.P., Dietrich, W.E., Brimhall, G.H., 2002. Weathering profiles, mass-balance analysis, and rates of solute loss: linkage between weathering and erosion in a small, steep catchment. Geol. Soc. Am. Bull. 114, 1143–1158.

Andrews, A., Godwin, C.I., Sinclair, A.J., 1984. Mixing line isochrons: a new interpretation of galena lead isotope data from southwestern British Columbia. Econ. Geol. 79, 919–932.

Andrews, D.M., Lin, H., Zhu, Q., Jin, L., Brantley, S.L., 2011. Soil carbon storage and dissolved organic carbon export in the Shale Hills Critical Zone Observatory. Vadose Zone J. 10, 943–954.

Barrett, P.M., Resing, J.A., Buck, N.J., Buck, C.S., Landing, W.M., Measures, C.I., 2012. The trace element composition of suspended particulate matter in the upper 1000 m of the eastern North Atlantic Ocean: A16N. Mar. Chem. 142–144, 41–53, http://dx.doi.org/10.1016/j.marchem.2012.07.006.

Blum, J.D., Erel, Y., 2004. Radiogenic isotopes in weathering and hydrology. In: Drever, J.I. (Ed.), Treatise of Geochemistry, vol. 5. pp. 365–393.

Brantley, S.L., Holleran, M., Jin, L., Bazilevskaya, E., 2013. Probing deep weathering in the Shale Hills Critical Zone Observatory, Pennsylvania (U.S.A.): the hypothesis of nested chemical reaction fronts in the subsurface. Earth Surf. Process Landf. 38, 1280–1298.

Brantley, S.L., Lebedeva, M., 2011. Learning to read the chemistry of regolith to understand the critical zone. Annu. Rev. Earth Planet. Sci. 39, 387–416, http://dx.doi.org/10.1146/annurev-earth-040809-152321.

Brantley, S.L., White, A.F., 2009. Approaches to modeling weathered regolith. Rev. Mineral. Geochem. 70, 435–484.

Brantley, S.L., White, T.S., Ragnarsdottir, K.V., 2007. The critical zone: where rock meets life. Elements 3, 368.

Brimhall, G.H., Dietrich, W.E., 1987. Constitutive mass balance relations between chemical composition, volume, density, porosity, and strain in metosomatic hydrochemical systems: results on weathering and pedogenesis. Geochim. Cosmochim. Acta 51, 567–587.

Burkitt, A., Lester, P., Nickless, G., 1972. Distribution of heavy metals in the vicinity of an industrial complex. Nature 238, 327–328.

Caldeira, K., Morgan, M.G., Baldocchi, D., Brewer, P.G., Chen, C.T.A., Nabuurs, G.J., Nakicenovic, N., Robertson, G.P., 2004. A portfolio of carbon management options. In: Field, C.B., Raupach, M.R. (Eds.), The Global Carbon Cycle. Island Press, Washington, DC, USA, pp. 103–130.

Chow, T.J., Earl, J.L., 1972. Lead isotopes in North American coals. Science 176, 510–511.

Clarke, L.B., Sloss, L.L., 1992. Trace Elements—Emissions from Coal Combustion and Gasification. IEA Coal Research, London, pp. 111.

Cloquet, C., Carignan, J., Libourel, G., 2006. Isotopic composition of Zn and Pb atmospheric depositions in an urban/periurban area of northeastern France. Environ. Sci. Technol. 40, 6594–6600.

Conko, K.M., Rice, K.C., Kennedy, M.M., 2004. Atmospheric wet deposition of trace elements to a suburban environment, Reston, Virginia, USA. Atmos. Environ. 38, 4025–4033.

Cumming, G.L., Richards, J.R., 1975. Ore lead isotope ratios in a continuously changing Earth. Earth Planet. Sci. Lett. 28, 155–171.

Cumming, G.L., Kesler, S.E., Krstic, D., 1979. Isotopic composition of lead in Mexican mineral deposits. Econ. Geol. 74, 1395–1407.

Doe, B.R., Delevaux, M.H., 1972. Source of lead in southeast Missouri galena ores. Econ. Geol. 67, 409–425.

Drivas, P., Bowers, T., Yamartino, R., 2011. Soil mixing depth after atmospheric deposition. I. Model development and validation. Atmos. Environ. 45, 4133–4140.

Dudka, S., Adriano, D.C., 1997. Environmental impacts of metal ore mining and processing: a review. J. Environ. Qual. 26, 590–602.

Duffy, C.J., Cusumano, J.M., 1998. A low-dimensional model for concentration-discharge in groundwater-stream systems. Water Resour. Res. 34, 2235–2247.

Edgington, D.N., Robbins, J.A., 1976. Records of lead deposition in Lake Michigan sediments since 1800. Environ. Sci. Technol. 10, 266–274.

Eggert, G.G., 1994. The Iron Industry in Pennsylvania. Pennsylvania Historical Association, Harrisburg 98 pp.

Eisenreich, S.J., Metzer, N.A., Urban, N.R., Robbins, J.A., 1986. Response of atmospheric lead to decreased use of lead in gasoline. Environ. Sci. Technol. 20, 171–174.

Erel, Y., Harlavan, Y., Blum, J.D., 1994. Lead isotope systematics of granitiod weathering. Geochim. Cosmochim. Acta 58, 5299–5306.

Fernandez, C., Monna, F., Labanowski, J., Loubet, M., van Oort, F., 2008. Anthropogenic lead distribution in soils under arable land and permanent grassland estimated by Pb isotopic compositions. Environ. Pollut. 156, 1083–1091.

Folk, R.L., 1960. Peterography and origin of the Tuscarora, Rose Hill, and Keefer Formations, Lower and Middle Silurian of eastern west Virginia. J. Sediment. Petrol. 30, 1–58.

FOREGS, 2010. Geochemical Atlas of Europe. Available from: http://www.gtk.fi/publ/foregsatlas/

Galloway, J.N., Thornton, J.D., Norton, S.A., Volchok, H.L., McLean, R.A.N., 1982. Trace metals in atmospheric deposition: a review and assessment. Atmos. Environ. 16, 1677–1700.

Gaillardet, J., Viers, J., Dupre, B., 2004. Trace elements in river waters. In: Drever, J.I. (Ed.), Treatise of Geochemistry, vol. 5. pp. 225–272.

Gaines, K.P., Eissenstat, D., Lin, H., 2013. Patterns in tree water extraction depth at the Susquehanna Shale Hills Critical Zone Observatory in central Pennsylvania. In: EAS Annual Meeting, Minneapolis, Minnesota, August 4–9.

Gardner, T.W., Ritter, J.B., Shuman, C.A., Bell, J.C., Sasowsky, K.C., Pinter, N., 1991. A periglacial stratified slope deposit in the valley and ridge province of central Pennsylvania USA: sedimentology, stratigraphy, and geomorphic evolution. Permafr. Periglac. Process 2, 141–162.

Geagea, M.L., Stille, P., Gauthier-Lafaye, F., Millet, M., 2008. Tracing of industrial aerosol sources in an urban environment using Pb, Sr, and Nd isotopes. Environ. Sci. Technol. 42, 692–698.

Graney, J.R., Halliday, A.N., Keeler, G.J., Nriagu, J.O., Robbins, J.A., Norton, S.A., 1995. Isotopic record of lead pollution in lake sediments from the northeastern United States. Geochem. Cosmochim. Acta 59, 1715–1728.

Gulson, B.L., Tiller, K.G., Mizon, K.J., Merry, R.H., 1981. Use of lead isotope ratios in soils to identify the source of lead contamination near Adelaide, South Australia. Environ. Sci. Technol. 15, 691–696.

Gunnesch, K.A., Baumann, A., Gunnesch, M., 1990. Lead isotope variations across the central Peruvian Andes. Econ. Geol. 85, 1384–1401.

Hanan, B.B., Schilling, J.-G., 1989. Easter microplate evolution: Pb isotope evidence. J. Geophys. Res. 94, 7432–7448, http://dx.doi.org/10.1029/JB094iB06p07432.

Hanan, B.B., Blichert-Toft, J., Pyle, D., Christie, D., 2004. Contrasting origins of the upper mantle MORB source revealed by Hf and Pb isotopes from the Australian-Antarctic Discordance. Nature 432, 91–94, http://dx.doi.org/10.1038/nature03026.

Hanan, B.B., Shervais, J.W., Vetter, S.K., 2008. Yellowstone plume-continental lithosphere interaction beneath the Snake River Plain. Geology 36, 51–54, http://dx.doi.org/10.1130/G23935A.1.

He, Q., Walling, D.E., 1997. The distribution of fallout 137Cs and 210Pb in undisturbed and cultivated soils. Appl. Radiat. Isot. 48, 677–690.

Herndon, E.M., Jin, L., Brantley, S.L., 2011. Soils reveal widespread manganese enrichment from industrial inputs. Environ. Sci. Technol. 45, 241–247.

Heyl, A.V., Landis, G.P., Zartman, R.E., 1974. Isotopic evidence for the origin of Mississippi Valley-type mineral deposits: a review. Econ. Geol. 69, 992–1006.

Hissler, C., Stille, P., Krein, A., Geagea, M.L., Perrone, T., Probst, J.-L., Hoffmann, L., 2008. Identifying the origins of local atmospheric deposition in the steel industrial basin of Luxembourg using the chemical and isotopic composition of the lichen *Xanthoria parietina*. Sci. Total Environ. 405, 338–344.

Jackson, M.L., 1967. Soil Chemical Analysis. Prentice-Hall, Inc., Englewood, NJ 498 pp.

Jin, L., Andrews, D., Holmes, G., Lin, H., Brantley, S.L., 2011a. Opening the "Black Box": water chemistry reveals hydrological controls on weathering in the Susquehanna Shale Hills Critical Zone Observatory. Vadose Zone J. 10, 928–942.

Jin, L., Ravella, R., Ketchum, B., Bieman, P.R., Heaney, P., White, T., Brantley, S.L., 2010. Mineral weathering and elemental transport during hillslope evolution at the Susquehanna/Shale Hills Critical Zone Observatory. Geochim. Cosmochim. Acta 74, 3669–3691.

Jin, L., Rother, G., Cole, D., Mildner, D., Duffy, C., Brantley, S.L., 2011b. Characterization of deep weathering and nanoporosity development in shale – a neutron study. Am. Mineral. 96, 498–512.

Kaste, J.M., Friedland, A.J., Sturup, S., 2003. Using stable and radioactive isotopes to trace atmospherically deposited Pb in montane forest soils. Environ. Sci. Technol. 37, 3560–3567.
Kaste, J.M., Heimsath, A.M., Bostick, B.C., 2007. Short-term soil mixing quantified with fallout radionuclides. Geology 35, 243–246.
Kelly, A.E., Reuer, M.K., Goodkin, N.F., Boyle, E.A., 2009. Lead concentrations and isotopes in corals and water near Bermuda, 1780–2000. Earth Planet. Sci. Lett. 283, 93–100.
Kim, G., Hussain, N., Scudlark, J.R., Church, T.M., 2000. Factors influencing the atmospheric depositional fluxes of stable Pb, ^{210}Pb, and ^{7}Be into Chesapeake Bay. J. Atmos. Chem. 36, 65–79.
Klaminder, J., Renberg, I., Binder, R., 2003. Isotopic trends and background fluxes of atmospheric lead in northern Europe: analyses of three ombrotrophic bogs from south Sweden. Glob. Biogeochem. Cycles 17, 1019, http://dx.doi.org/10.1029/2002GB001921.
Komarek, M., Ettler, V., Chrastny, V., Mihaljevic, M., 2008. Lead isotopes in environmental sciences: a review. Environ. Int. 34, 562–577.
Konter, J.G., Jackson, M.G., 2012. Large volumes of rejuvenated volcanism in Samoa: evidence supporting a tectonic influence on late-stage volcanism. Geochem. Geophys. Geosyst. 13, Q0AM04, http://dx.doi.org/10.1029/2011GC003974.
Lantzy, R.J., Mackenzie, F.T., 1979. Atmospheric trace metals: global cycles and assessment of man's impact. Geochem. Cosmochim. Acta 43, 511–525.
Lima, A.L., Bergquist, B.A., Boyle, E.A., Reuer, M.K., Dudas, F.O., Reddy, C.M., Eglinton, T.I., 2005. High-resolution historical records from Pettaquamscutt River basin sediments: 2. Pb isotopes reveal a potential new stratigraphic marker. Geochem. Cosmochim. Acta 69, 1813–1824.
Lin, H., Kogelmann, W., Walker, C., Bruns, M.A., 2006. Soil moisture patterns in a forested catchment: a hydropedological perspective. Geoderma 131, 345–368.
Lin, H.S., 2006. Temporal stability of soil moisture spatial pattern and subsurface preferential flow pathways in the Shale Hills Catchment. Vadose Zone J. 5, 317–340.
Lynch, J.A., 1976. Effects of Antecedent Soil Moisture on Storm Hydrographs. Pennsylvania State University, University Park.
Lynch, J.A., Corbett, E.S., 1985. Source-area variability during peak flow. In: Jones, E.B., Ward, T.J. (Eds.), J. Irrig. Drain. Div. Am. Soc. Civ. Eng. Watershed Management in the 1980, ASCE, Reston, VA, pp. 300–307.
Ma, L., Chabaux, F., Pelt, E., Blaes, E., Jin, L., Brantley, S., 2010. Regolith production rates calculated with uranium-series isotopes at Susquehanna/Shale Hills Critical Zone Observatory. Earth Planet. Sci. Lett. 297, 211–225.
Ma, L., Chabaux, F., West, N., Kirby, E., Jin, L., Brantley, S.L., 2013. Regolith production and transport in the Susquehanna Shale Hills Critical Zone Observatory, Part 1: Insights from U-series isotopes. J. Geophys. Res. Earth Surf. 118, 722–740, http://dx.doi.org/10.1002/jgrf.20037.
Ma, L., Jin, L., Brantley, S.L., 2011a. Controls of mineralogy and slope aspect on REE release and fractionation during shale weathering in the Susquehanna/Shale Hills Critical Zone Observatory. Chem. Geol. 290, 31–49.
Ma, L., Jin, L., Brantley, S.L., 2011b. Geochemical behaviors of different element groups during shale weathering at the Susquehanna/Shale Hills Critical Zone Observatory. Appl. Geochem. 26, S89–S93.
Mackay, A.K., Taylor, M.P., Munksgaard, N.C., Hudson-Edwards, K.A., Burn-Nunes, L., 2013. Identification of environmental lead sources and pathways in a mining and smelting town: Mount Isa, Australia. Environ. Pollut. 180, 304–311.
Marcantonio, F., Zimmerman, A., Xu, Y., Canuel, E., 2002. A Pb isotope record of mid-Atlantic US atmospheric Pb emissions in Chesapeake Bay sediments. Mar. Chem. 77, 123–132.
Markus, J., McBratney, A.B., 2001. A review of the contamination of soil with lead II. Spatial distribution and risk assessment of soil lead. Environ. Int. 27, 399–411.
Miller, E.K., Friedland, A.J., 1994. Lead migration in forest soils: response to changing atmospheric inputs. Environ. Sci. Technol. 28, 662–669.
Naithani, K.J., Baldwin, D., Gaines, K., Lin, H., Eissenstat, D.M., 2013. Spatial distribution of tree species governs the spatio-temporal interaction of leaf area index and soil moisture across a forested landscape. PLoS ONE, http://dx.doi.org/10.1371/journal.pone.0058704.
National Oceanographic and Atmospheric Administration (NOAA), 2007. U.S. Divisional and Station Climatic Data and Normals: Asheville, North Carolina U.S. Department of Commerce, National Oceanic and Atmospheric Administration, National Environmental Satellite Data and Information Service, National Climatic Data Center, In: http://cdo.ncdc.noaa.gov/CDO/cdo.
Nriagu, J.O., Pacyna, J.M., 1988. Quantitative assessment of worldwide contamination of air, water and soils by trace metals. Nature 333, 134–139.
Qu, T., Duffy, C.J., 2007. A semi-discrete finite volume formation for multiprocess watershed simulation. Water Resour. Res. 43 , http://dx.doi.org/10.1029/2006WR005752.
Rauch, J.N., Pacyna, J.M., 2009. Earth's global Ag, Al, Cr, Cu, Fe, Ni, Pb, and Zn cycles. Glob. Biogeochem. Cycles 23, GB2001, http://dx.doi.org/10.1029/2008GB003376.
Reuer, M.K., Weiss, D.J., 2002. Anthropogenic lead dynamics in the terrestrial and marine environment. Phil. Trans. R. Soc. Lond. A 360, 2889–2904.
Roux, G.L., Aubert, D., Stille, P., Krachler, M., Kober, B., Cheburkin, A., Bonani, G., Shotyk, W., 2005. Recent atmospheric Pb deposition at a rural site in southern Germany assessed using a peat core and snowpack, and comparison with other activities. Atmos. Environ. 39, 6790–6801.
Steinnes, E., Friedland, A.J., 2005. Lead migration in Podzolic soils from Scandinavia and the United States of America. Can. J. Soil Sci. 85, 291–294.
Taylor, M.P., Hudson-Edwards, K.A., Mackay, A.K., Holz, E., 2010. Soil Cd, Cu, Pb and Zn contaminants around Mount Isa city, Queensland, Australia: potential sources and risks to human health. Appl. Geochem. 25 (6) 841–855.
Thompson, T.B., Beaty, D.W., 1990. Geology and origin of ore deposits in the Leadville district, Colorado: Part II. Oxygen, hydrogen, carbon, sulfur, and lead isotopic data and development of a genetic model. Econ. Geol. Monogr. 7, 156–179.
Todt, W., Cliff, R., Hanser, A., Hofmann, A.W., 1996. Evaluation of a 202Pb–205Pb double spike for high precision lead isotope analysis. In: Basu, A., Hart, S.R. (Eds.), Earth Processes: Reading the Isotopic Code, Geophys. Monogr. Ser., vol. 95. AGU, Washington, DC, pp. 429–437, http://dx.doi.org/10.1029/GM095p0429.
Watmough, S.A., Hutchison, T.C., Dillon, P., 2004. Lead dynamics in the forest floor and mineral soil in south-central Ontario. Biogeochemistry 71, 43–68.
Weis, D., et al., 2006. High-precision isotopic characterization of USGS reference materials by TIMS and MC-ICP-MS. Geochem. Geophys. Geosyst. 7, Q08006, http://dx.doi.org/10.1029/2006GC001283.
West, N., Kirby, E., Bierman, P.R., Rood, D.H., 2011. Preliminary estimates of regolith generation and mobility in the Susquehanna Shale Hills Critical Zone Observatory, PA, using meteoric 10Be. Appl. Geochem. 26, S146–S148.
West, N., Kirby, E., Bierman, P., Slingerland, R., Ma, L., Rood, D., Brantley, S., 2013. Regolith production and transport at the Susquehanna Shale Hills Critical Zone Observatory: Part 2. Insights from meteoric 10Be. J. Geophys. Res. Earth Surf., http://dx.doi.org/10.1002/jgrf.20121.
White, W.M., Albarède, F., Telouk, P., 2000. High-precision analysis of Pb isotope ratios by multi-collector ICP-MS. Chem. Geol. 167, 257–270, http://dx.doi.org/10.1016/S0009-2541(99)00182-5.
Yesavage, T.A., Fantle, M.S., Vervoort, J., Mathur, R., Jin, L., Liermann, L.J., Brantley, S.L., 2012. Fe cycling in the Shale Hills Critical Zone Observatory, Pennsylvania: an analysis of biogeochemical weathering and Fe isotope fractionation. Geochim. Cosmochim. Acta 99, 18–38.